Journal of Catalysis 354 (2017) 46–60

Contents lists available at ScienceDirect

Journal of Catalysis

journal homepage: www.elsevier.com/locate/jcat

The role of electronic metal-support interactions and its temperature dependence: CO adsorption and CO oxidation on Au/TiO_2 catalysts in the presence of TiO_2 bulk defects

Y. Wang [a], D. Widmann [a], M. Heenemann [b], T. Diemant [a], J. Biskupek [d], R. Schlögl [b,c], R.J. Behm [a,*]

[a] Institute of Surface Chemistry and Catalysis, Ulm University, D-89069 Ulm, Germany
[b] Department of Inorganic Chemistry, Fritz-Haber-Institut der Max-Planck-Gesellschaft, D-14195 Berlin, Germany
[c] Department of Heterogeneous Reactions, Max-Planck-Institut für Chemische Energiekonversion, D-45470 Mülheim an der Ruhr, Germany
[d] Central Facility of Electron Microscopy, Group of Materials Science, Ulm University, D-89069 Ulm, Germany

ARTICLE INFO

Article history:
Received 19 June 2017
Revised 27 July 2017
Accepted 28 July 2017
Available online 31 August 2017

Keywords:
Au/TiO_2
CO oxidation
CO adsorption
Electrical conductivity
Bulk defects
Electronic metal-support interactions (EMSIs)
Kinetic measurements
IR

ABSTRACT

We report results of a comprehensive study on the effect of bulk defects on the catalytic behavior of Au/TiO_2 catalysts in the CO oxidation reaction, combining quantitative information on the amount of surface and bulk defects from *in situ* non-contact electrical conductivity measurements after pretreatment and during reaction with information on the electronic/chemical state of the Au nanoparticles (NPs) provided by *in situ* IR spectroscopy. Treating the catalyst in strongly reducing atmosphere (10% CO/90% N_2) at 400 °C results in a distinct increase in electrical conductivity, indicative of the formation of defects (oxygen vacancies), which are stable at 80 °C in N_2. Long-term kinetic measurements performed at 80 °C show a distinctly lower activity of the bulk reduced catalyst, which increases slowly with time on stream, directly correlated with the decreasing abundance of bulk defects. The detrimental effect of bulk defects on the CO oxidation activity is shown to originate from the lowered CO adsorption strength and hence very low CO_{ad} coverage on the Au NPs due to electronic metal-support interactions (EMSIs) induced by the presence of TiO_2 bulk defects, in good agreement with our recent proposal (Wang et al., ACS Catal. 7 (2017) 2339). For reaction at −20 °C, EMSIs lead to a promoting effect on the CO oxidation, pointing to a change in the dominant reaction mechanism, away from the Au-assisted Mars-van Krevelen mechanism dominant at 80 °C. The role of EMSIs in the CO oxidation reaction and its temperature dependence is discussed in detail.

1. Introduction

Metal – support interactions are well known to play an important and often decisive role for the catalytic performance of supported metal catalysts, in particular for catalysts supported on reducible (oxide) supports [1–6]. Tauster introduced the term *strong metal – support interactions (SMSIs)* [7], which according to his definition refers to a specific strongly bonding interaction between support and metal nanoparticles (NPs) that is created upon treating the catalyst in a reducing atmosphere. These interactions may result in a variety of effects such as masking parts of the metal surface, by overgrowth of the metal surface with the reduced oxide, the formation of specific contact zones with enhanced catalytic performance or spreading of the metal [1]. They were attributed to the formation of less positively charged cations, such as Ti^{3+} in the case of TiO_2, at the surface of the support upon reducing treatment and their specific interactions with the metal NPs. Recently, electronic interactions involving a distinct modification of the electronic properties of the metal NPs, in this case for Pt NPs on CeO_2, were introduced as yet another type of SMSIs [5,8]. These electronic metal-support interactions (EMSIs) were demonstrated to significantly improve, e.g., the ability of a Pt/CeO_2 catalyst to dissociate the O-H bonds in water in the water gas shift reaction to produce H_2.

While these examples refer to the direct bonding interaction at the interface, one may also envision that deeper lying defects, e.g., bulk vacancies in oxide supports, may affect the catalytic performance of a catalyst via electronic interactions. Freund and coworkers had shown, e.g., that the CO adsorption properties of very small Au NPs on a MgO film, depended sensitively on the thickness of the oxide film [9–11]. They explained this by an increasing probability for electron transfer from the metal oxide support to the electronegative Au NPs with decreasing film thickness, the size of the

* Corresponding author.
E-mail address: juergen.behm@uni-ulm.de (R.J. Behm).

http://dx.doi.org/10.1016/j.jcat.2017.07.029
0021-9517/

Au NPs [9,10] and increasing film conductivity due to defects/doping [10,12,13]. The influence of charging on the catalytic activity of small supported metal clusters was convincingly demonstrated in previous studies on surface deposited mass selected metal clusters [14].

The possible influence of deeper lying bulk defects on the catalytic performance of supported metal catalysts, mediated via electronic metal – support interactions, is topic of an ongoing study in our laboratory, in which we aim at a fundamental understanding of such effects using oxide supported Au catalysts as model system. Here we report results of a comprehensive study on the influence of bulk defects in the CO oxidation reaction on Au/TiO_2 catalysts, combining kinetic measurements with *in situ* IR spectroscopy and electrical conductivity measurements. The influence of bulk defects is identified by comparing the CO adsorption and reaction properties of a Au/TiO_2 catalyst in the presence and absence of oxygen bulk vacancies, which were annihilated or created by pretreatment in a strongly oxidizing (O400, 10% O_2/90% N_2) or strongly reducing (CO400, 10% CO/90% N_2) atmosphere at 400 °C, respectively. To distinguish between bulk defects and surface vacancies and their re-oxidation, adsorption/reaction measurements were performed at two different temperatures, 80 °C and −20 °C, where re-oxidation of bulk vacancies is slow but possible (80 °C) or essentially inhibited (−20 °C). First preliminary results of this study were reported recently [15].

Before presenting and discussing the results of our study, we will briefly summarize previous findings relevant for the understanding of this study. From their similarity with reducible oxides supported platinum group metal (PGM) catalysts, SMSI effects would be observed also for the corresponding supported Au catalysts such as Au/TiO_2. Previous studies found no indications for encapsulation of the Au NPs by a reduced oxide layer upon high temperature annealing in vacuum or under reducing atmospheres [3,16]. It was proposed that the lack of such an encapsulation of the Au NPs in Au/TiO_2 catalysts is due to the weaker interaction of Au with reduced TiO_{2-x} compared to that of Pt. On the other hand, Tang et al. reported the observation of partial encapsulation of Au nanoparticles the support during oxidative pretreatment and a pronounced stabilization of the metal nanoparticles against sintering for a Au nanoparticle catalyst supported on hydroxyapatite (HAP) [17].

While little is known about the role of bulk oxygen vacancies, much more attention has been devoted to surface vacancies, whose role in the CO oxidation reaction was studied in detail. In a series of temporal analysis of products (TAP) reactor studies we provided convincing evidence that they participate in the CO oxidation reaction via a Au-assisted Mars – van Krevelen mechanism, involving the Au-assisted formation of surface lattice oxygen vacancies at the perimeter sites of the Au-TiO_2 interface by reaction with adsorbed CO and the subsequent replenishment of these vacancies by reaction with molecular oxygen [18,19]. This mechanism was proposed as dominant mechanism for CO oxidation on Au catalysts supported on reducible oxides at ambient temperature and above [18–23].

Maeda et al. followed the electrical conductivity during CO oxidation on a Au/TiO_2 catalyst pretreated in an oxidizing atmosphere [24]. They observed a distinct increase in conductivity of the catalyst upon exposure to the reaction gas mixture ($CO:O_2 = 2:1$, 50 mbar, 200 °C). A significantly higher increase was observed upon exposure to CO at 200 °C. In both cases, however, the authors claimed that vacancy formation was limited to the creation of surface vacancies. Based on these results they concluded that surface vacancies generated during the CO oxidation stabilize adsorbed O_2 and thus activate O_2 for the reaction [24].

A number of model studies performed on single crystal TiO_2 or ultrathin TiO_2 films decorated with Au nanoparticles reported that surface defects act as preferential nucleation sites for Au NP growth and stabilize them against sintering [25–30]. Furthermore, from the red-shift of Au-CO_{ad} IR band absorption frequency and based on theoretical calculations they proposed an electron transfer from surface defect sites on reduced TiO_{2-x} to the Au NPs, resulting in electron rich and often more active Au species [27–30]. Furthermore, Goodman concluded that by re-oxidizing previously reduced TiO_{2-x} thin film substrates or highly disperse supports in oxidizing atmospheres, the metal – support interaction can be reversed back to the original state after oxidizing pretreatment [31].

In the following we will, after a brief description of the Au/TiO_2 catalyst and its pretreatment as well as the experimental set-ups and procedures, first describe results of *ex situ* catalyst characterization before and after reaction by transmission electron microscopy (TEM) and X-ray photoelectron spectroscopy (XPS). Next we will present results of kinetic, *in situ* electrical conductivity and *in situ* IR spectroscopy measurements on the influence of bulk defects on the CO oxidation and CO adsorption characteristics, which was identified by comparing the adsorption/reaction characteristics of two catalyst samples from the same batch. The two catalysts were pretreated differently, one in oxidizing and one in reducing atmosphere at elevated temperature. Overall, these results are expected to provide detailed insight in the role of bulk oxygen vacancies in the CO oxidation reaction on supported Au catalysts, and also into the nature of the reaction mechanism for CO oxidation on Au/TiO_2 catalysts at temperatures below 0 °C, which was proposed [19,32] to differ from the Au-assisted Mars-van Krevelen mechanism dominant for Au catalysts supported on reducible oxides above room temperature [18,20–23]. The main conclusions derived from these results will finally be summarized.

2. Experimental section

2.1. Au/TiO_2 catalyst and pretreatment

For the experiments we used a commercially available Au/TiO_2 catalyst (AURO*lite*™, supplied by STREM Chemicals) prepared via deposition precipitation, with a Au loading of 1.0 wt%. P25 (Degussa AG) was used as TiO_2 support. The overall concentration of Na^+ and Cl^- in the catalyst is below 1500 ppm according to the supplier. Although the catalyst was already calcined before by the supplier, we pretreated it additionally *in situ* prior to all measurements in order to remove the majority of residual surface species such as hydrocarbons, moisture etc., which may have originated from exposure to air. For that reason the Au/TiO_2 catalyst was first dried *in situ* in a flow of 20 Nml·min^{-1} N_2 at 100 °C overnight (ca. 17 h) in order to obtain a low and constant level of adsorbed water and OH-groups on the catalyst surface, followed by *in situ* pretreatment at 400 °C for 30 min in either oxidizing (O400, 10% O_2/90% N_2, 20 Nml·min^{-1}) or reducing (CO400, 10% CO/90% N_2, 20 Nml·min^{-1}) atmosphere. After the respective pretreatment, the catalyst was cooled down to the desired reaction temperature in a flow of 20 Nml·min^{-1} N_2. For pretreatment as well as for subsequent reaction high purity gases from Westfalen AG were used (CO 4.7, O_2 5.0, N_2 6.0). Additionally, all gases were passed through an in-line water filter (Agilent, CP17971) before entering the reactor to prevent further insertion of water, and thus adsorption and accumulation of water on the catalyst surface during pretreatment and/or reaction.

2.2. Catalyst characterization

The mean Au NP size and the Au particle size distribution after both pretreatments and after reaction were evaluated from trans-

mission electron microscopy images (JEOL JEM 1400 and FEI Titan 80-300 microscopes). The Au/TiO_2 catalyst samples were dispersed in ethanol (ultrasound bath) and drop casted to holey carbon films. From the evaluation of at least 600 Au NPs for each sample, and assuming half-spherical Au NPs with $1.15 \cdot 10^{15}$ Au atoms·cm^{-2}, the dispersion of Au NPs (D_{Au}) was calculated according to:

$$D_{Au} = 6 \times \frac{v_m/a_m}{d_{VA}} = 6 \times \frac{v_m \times \sum_i n_i d_i^2}{a_m \times \sum_i n_i d_i^3} \quad (1)$$

Here v_m is the volume occupied by an Au atom in the bulk metal, a_m is the area occupied by a surface atom, d_{VA} is the volume-area mean diameter, d_i is the diameter of half-spherical particles, and n_i is the number of particles with diameter d_i.

The oxidation state of Au and Ti as well as their atomic ratios in the topmost layers of the Au/TiO_2 catalyst, and in particular any differences therein after oxidizing or reducing pretreatment, were monitored by *ex situ* X-ray photoelectron spectroscopy (XPS) measurements (PHI 5800 ESCA), using monochromatized Al Kα radiation (1486.6 eV). The measurements were performed at an emission angle of 45° using analyser pass energies of 93.9 and 29.35 eV for survey and detail spectra, respectively. Core level spectra of C 1s, O 1s, Au 4f and Ti 2p were recorded. Shirley background subtraction and peak fitting were performed using the CasaXPS software. In order to correct for surface charging effects, the binding energies of all spectra were calibrated using the Ti $2p_{3/2}$ peak at a position of 459.2 eV as reference [33].

The TiO_2 support structure of the catalyst after different pretreatments was characterized by X-ray diffraction (XRD), performed on a Siemens D5000 and a STOE Stadi-P diffractometer using Cu Kα radiation (λ = 0.154 nm). The ratio of anatase/rutile phase was estimated by comparing the relative intensities of the diffraction peaks at 25.4° (anatase(1 0 1)) and 27.5° (rutile(1 1 0)).

2.3. Kinetic measurements (CO oxidation)

Catalytic activities of the Au/TiO_2 catalysts for the continuous CO oxidation after *in situ* pretreatment were determined in a micro-reactor at atmospheric pressure. For direct access to the reaction kinetics and to obtain information on the deactivation of the catalysts with time on stream (TOS), isothermal measurements were performed under differential reaction conditions, with CO conversions (X_{CO}, see Eq. (2)) below 20%. To realize such low conversions, the catalysts were diluted with α-Al_2O_3, which under present reaction conditions is inactive for CO oxidation. A total of ca. 80 mg of the diluted catalysts, with dilutions of 1:80 and 1:2, were used for measurements at 80 °C and −20 °C, respectively. From the CO conversion, the Au mass normalized reaction rates (R_{Au}) were calculated according to Eq. (3). The CO conversion is determined either from the (relative) CO consumption or from the corresponding CO_2 formation (Eq. (2)):

$$X_{CO} = \frac{\dot{n}_{CO,in} - \dot{n}_{CO,out}}{\dot{n}_{CO,in}} = \frac{\dot{n}_{CO2,out}}{\dot{n}_{CO,in}} \quad (2)$$

$$R_{Au} = \frac{X_{CO} \times \dot{n}_{CO,in}}{m_{Au}} \quad (3)$$

Here m_{Au} is the Au mass present in the catalyst bed and $\dot{n}_{CO,in}$ and $\dot{n}_{CO,out}$ are the molar flows of CO into/out of the reactor. Considering also the Au dispersion of the catalysts (D_{Au}) obtained from TEM imaging, and the molar mass of Au (M_{Au}), we also calculated turnover frequencies (TOFs), which represent the activity for CO oxidation normalized to the overall number of surface Au atoms of the Au NPs:

$$TOF = \frac{R_{Au} \times M_{Au}}{D_{Au}} \quad (4)$$

All measurements were performed with a total gas flow of 60 Nml·min^{-1} in a reaction atmosphere containing 1% CO, 1% O_2, 98% N_2. To achieve dry reaction conditions, all reaction gases were passed through an in-line water filter, and their water content was monitored by an in-line water sensor (Alpha-moisture, Model AMT) before entering the micro-reactor. This resulted in water contents of ≤0.2 ppm in the reaction gas feed. Hence, water accumulation on the catalyst surface, and any effects therefrom on the activity/stability of the catalyst can essentially be excluded. Influent and effluent gases were analyzed by on-line gas chromatography using H_2 as carrier gas (DANI, GC 86.10HT), with a time resolution of about 16 min. Since it takes at least 2–3 min to reach a stable gas phase composition in the reactor after starting the reaction by replacing N_2 with the reactive gas mixture, the first sample of the reaction gas atmosphere was always collected 10 min after switching to the reaction gas mixture. The initial activity in all measurements thus refers to that after 10 min TOS. Although kinetic information in the first 10 min are lost in this approach, this procedure is mandatory in order to obtain a reproducible initial activity, which is essential for the determination of the catalysts deactivation with time on stream and for a reliable comparison between different measurements.

2.4. In situ electrical conductivity measurements: microwave cavity perturbation technique

The contact-free electrical conductivity of Au/TiO_2 was measured employing the microwave cavity perturbation technique [34–36]. This measurement is based on the principle that the electromagnetic field inside a microwave cavity is modified by placing a sample therein, which causes a shift of the resonance frequency and a decrease of the quality factor [34]. The complex permittivity ($\varepsilon = \varepsilon_1 + i\varepsilon_2$) describes this dielectric response of the sample. In the experiment we applied the Smith chart analysis and the transmission line theory to obtain the frequency and quality factor of the microwave cavity with and without Au/TiO_2 [37]. The imaginary part of the complex permittivity ε_2 is calculated from the changes in the quality factor and is further related to the microwave conductivity σ, which is given in effective values.

The measurements were performed in a cylindrical gold-plated S-band brass cavity. We used the first transverse magnetic mode (TM_{010}) at an empty resonance frequency of about 3.26 GHz. The plug-flow reactor was located in the electric field maximum and connected with a gas supply (Bronkhorst, El-Flow). The reactor tube was filled with Au/TiO_2 (100–200 µm sieve fraction) to a bed length of 4 mm, corresponding to a weight of 29 mg. A total gas flow of 20 ml·min^{-1} was applied. The measurement was started in pure N_2 and the sample was heated to 100 °C with a heating rate of 25 °C·min^{-1} and a dwell time of 90 min. Then, the temperature was increased to 400 °C and the pretreatment was performed in 5% O_2/95% N_2 (O400) and 5% CO/95% N_2 (CO400), respectively. After this pretreatment the temperature was decreased to 80 °C with a cooling rate of 25 °C·min^{-1} and a dwell time of 60 min in N_2. Afterwards, the catalyst was exposed to a reaction gas mixture of 1% CO, 1% O_2 and 98% N_2 for 240 min. We analyzed the effluent gas flow with an on-line gas chromatograph (Agilent 7890, equipped with a poraplot and a molecular sieve type column connected to a thermal conductivity detector and a DB1 column connected to a flame ionization detector). From experimental reasons, these measurements were only possible at ambient temperature and above. It should be noted that these powder measurements cannot distinguish between conductivity of electrons close to the surface and through the central parts of the TiO_2 particles. Further details of the microwave cavity perturbation technique can be found in Refs. [34,36,38].

2.5. In situ infrared spectroscopy (DRIFTS) measurements

In situ infrared spectroscopy measurements were performed in a DRIFTS (Diffuse Reflectance Infrared Fourier Transform Spectroscopy) configuration with a Nicolet 6700 spectrometer, equipped with a MCT narrow band detector and a commercial *in situ* reaction cell unit from Harricks (HV-DR2). For sample preparation the sample holder of the reaction cell was first filled with pure α-Al_2O_3, on which a top layer (about 1 mm) of the diluted catalyst was placed (ca. 40–50 mg, with dilutions of 1:10 and 1:2 for reactions at 80 °C and −20 °C, respectively). During pretreatment as well as during reaction all (reaction) gas mixtures were passed from top to bottom through the catalyst bed.

Prior to the reaction measurements, background spectra were recorded on the freshly calcined catalysts at the reaction temperature in a flow of 60 Nml·min^{-1} pure N_2. Typically, fast scan spectra (consisting of 20 scans with an overall acquisition time of 15 s) were recorded at the beginning of the reaction (first 10 min), where significant changes on the catalyst surface including the formation of surface species are expected to occur. Afterwards, normal scan spectra (400 scans, overall acquisition time ca. 4 min per spectrum) were recorded to achieve a higher signal to noise ratio. The ratio between the single beam intensity measured during reaction (I_R) and during the previously recorded background (I_B) defines the relative diffuse reflectance (R, Eq. (5)), which describes the IR absorption by the surface species formed during reaction. This relative diffuse reflectance was further evaluated in Kubelka-Munk units (Eq. (6)), which are linearly related to the adsorbate concentration [39,40].

$$R = \frac{I_R}{I_B} \tag{5}$$

$$KMU = \frac{(1-R)^2}{2R} \tag{6}$$

The CO oxidation measurements in the DRIFTS set-up were carried out under reaction conditions identical to those used in kinetic measurements (1% CO, 1% O_2, 98% N_2; 60 Nml·min^{-1}). This is an essential requirement for a direct comparison between the build-up of surface species during reaction as determined by DRIFTS and the catalytic activity evaluated in kinetic experiments (see above). However, it should be noted that in the DRIFTS measurements usually higher amounts of the Au/TiO_2 catalyst had to be used in order to achieve a good signal to noise ratio in the absorption bands of adsorbed surface species. At 80 °C, for example, about 5 mg of the Au/TiO_2 catalyst had to be used in DRIFTS, while in kinetic measurements only ca. 1 mg of catalyst have been used (resulting in a steady-state CO conversion of about 10% in the latter experiments). This may result in non-differential reaction conditions for CO oxidation performed at 80 °C in the DRIFTS set-up, which may affect, e.g., the carbonate formation rate (from CO_2 product molecules), but is expected to have little effect on the CO adsorption. For measurements at −20 °C, in contrast, a rather similar amount of catalyst (ca. 20 mg) was used in both set-ups. This is due to the lower activity of the catalyst under these conditions, requiring a higher amount of catalyst in the kinetic measurements.

Considering that the position of the Au-CO_{ad} absorption band is quite sensitive to the oxidation state of the Au species [41,42], the position of the CO absorption band during these measurements can be used to gain more insight into the electronic properties of Au NPs. This approach was applied during reaction (CO adsorption in the presence of O_2) as well as during CO adsorption measurements (CO_{ad} in the absence of O_2, see below), similar to our approach in previous studies [15,43]. For the CO adsorption experiments, the catalyst was cooled down after *in situ* pretreatment to the desired adsorption temperature (80 °C or −20 °C), at which the gas feed was switched from pure N_2 (60 Nml·min^{-1}) to the CO adsorption gas mixture (1% CO, 99% N_2, 60 Nml·min^{-1}). The evolution of the Au-CO_{ad} (and the Ti-CO_{ad}) absorption band was monitored by DRIFTS with time on stream until it reached steady-state.

In all spectra presented throughout this study, contributions of the gas phase CO signal were already removed by subtracting a spectrum recorded on pure α-Al_2O_3 in CO containing atmosphere at the respective temperature from the region of gas phase CO (2040–2240 cm^{-1}) in the spectra recorded during reaction.

3. Results and discussion

3.1. Catalyst characterization

3.1.1. Au particle size (TEM)

From transmission electron microscopy (TEM) images of the Au/TiO_2 catalyst recorded directly after pretreatment, which are illustrated in Fig. 1, it is evident that there are no significant differences in the Au particle sizes after the two pretreatments, O400 and CO400, as we had already demonstrated previously [15]. Based on the corresponding particle size distributions (see Fig. 1a), the average Au particle diameters were determined to be 2.6 ± 0.8 nm and 2.4 ± 0.9 nm for the O400 and CO400 pretreated samples, respectively. Assuming half-spherical Au particles and $1.15 \cdot 10^{15}$ Au atoms·cm^{-2}, this corresponds to Au dispersions of 36% and 37% after O400 and CO400 pretreatment, respectively. Moreover, we also observed no significant differences in the Au particle shapes after both pretreatments, which has been examined by additional HR-TEM images (see also Fig. 1). These results are in good agreement with those reported recently by Saavedra et al., who used the same commercial Au/TiO_2 catalyst (AUROlite™ from STREM Chemicals) and also pretreated the catalyst either in an oxidizing (20% O_2) or in a reducing (20% H_2) atmosphere. Applying a combined infrared and Temkin analysis [44], these authors concluded that there is no difference in the Au particle size after different pretreatments (up to 16 h at 350 °C) [45]. Here it should be noted that the catalyst has already been calcined by the manufacturer before and that therefore Au NPs were already present on the fresh catalyst before our pretreatment. In addition, we also measured the Au particle sizes after CO oxidation at 80 °C for 1000 min for both pretreatments, showing no distinct deviations to the samples measured directly after pretreatment (see Fig. 1b). From these results, we can exclude that changes/differences in the Au particle size and shape contribute significantly to any differences in the catalytic behavior of the Au/TiO_2 catalysts after oxidizing and reducing pretreatment or changes therein during the CO oxidation reaction (at 80 °C).

3.1.2. Au and Ti oxidation state (XPS)

To check whether there is an overgrowth of the Au NPs by reduced TiO_{2-x} species and/or a change in the Au oxidation state due to metal-support interactions induced by the strongly reducing pretreatment at elevated temperature (CO400), as it has previously been reported for strong metal-support interactions (SMSIs) in platinum group metal/TiO_2 (PGM/TiO_2) catalysts [1,46,47], we also performed *ex situ* XPS measurements on the Au/TiO_2 catalysts after the different pretreatments. The measured spectra for the Au 4f, Ti 2p, C 1s and O 1s signals on an as received catalyst, after oxidizing (O400), and after reducing (CO400) pretreatment are shown in Fig. 2.

From these spectra it is obvious that there are essentially no differences between the samples after different pretreatments. In all cases, the binding energy of the Au $4f_{7/2}$ electrons is constant at 84.0 eV, which is characteristic for metallic Au^0 species [33,48]. At the same time there are minor contributions from oxidized Au

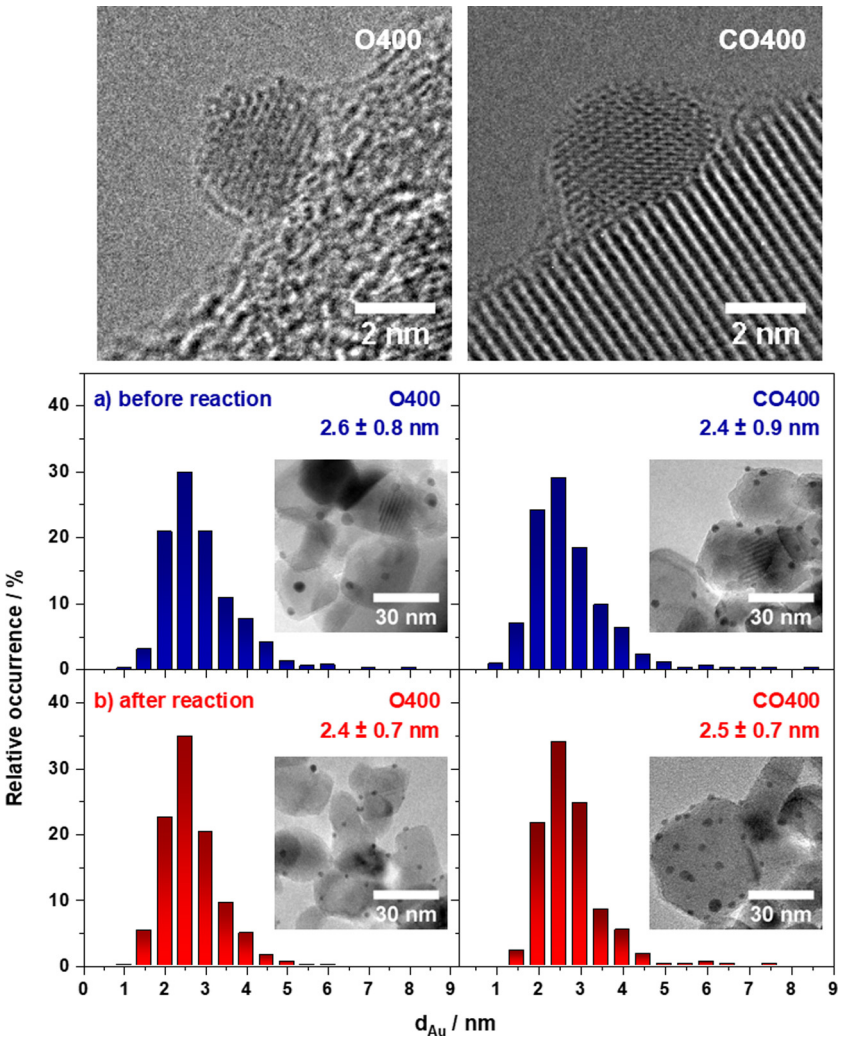

Fig. 1. Au particle size distributions and representative high resolution and overview TEM images of the Au/TiO_2 catalyst pretreated at 400 °C in oxidizing (O400, 10% O_2/90% N_2) or reducing (CO400, 10% CO/90% N_2) atmosphere (a) before and (b) after CO oxidation at 80 °C for 1000 min.

species, which appear at a higher binding energy of 85.9 eV [48,49]. The relative amount of the latter species differs, however, between the untreated, oxidized and reduced catalysts, yielding relative amounts of 6.6%, 9.9%, and 6.4%, respectively. Overall, the rather small amounts are in the limits of the accuracy of the fitting procedure. The higher Au^{3+} amount observed on the O400 pretreated sample may indicate some (surface) oxidation during this pretreatment, in agreement with findings of an irreversible oxide formation upon O400 pretreatment concluded in earlier TAP reactor studies [18,50]. Besides, we did not detect any significant contributions from Ti oxidation states other than Ti^{4+} [51], and also the atomic ratio of Au:Ti was essentially identical for the as received sample and for the two differently pretreated samples. The latter results seem to indicate that there is neither an encapsulation of the Au NPs by reduced TiO_{2-x} species (which would have resulted in a lower Au:Ti ratio), nor detectable changes in the Au or Ti oxidation state upon reducing pretreatment (CO400).

3.1.3. TiO_2 support structure (XRD)

The XRD patterns and the ratios of anatase: rutile phases of the different samples (see Fig. S1 and Table S1 in the Supporting Information) did not show any significant differences. Hence, there are essentially no changes in the structure of the TiO_2 support (P25) upon different pretreatments (O400, CO400).

3.2. Influence of TiO_2 bulk defects on the catalytic performance at 80 °C

3.2.1. Kinetic and in situ DRIFTS measurements

Next we determined the catalytic activity of the Au/TiO_2 catalyst for the CO oxidation after *in situ* pretreatment in oxidizing (O400: 10% O_2/90% N_2) or reducing (CO400: 10% CO/90% N_2) atmosphere under differential reaction conditions at a reaction temperature of 80 °C. As we have already reported recently [15], the catalyst is initially much more active after O400 pretreatment: After O400 and CO400, the initial TOFs for the CO oxidation on Au/TiO_2 are 4.1 s^{-1} and 1.7 s^{-1}, respectively (see Fig. 3). Note that the measured rates represent an average over the particle size distribution. For the pre-oxidized sample, this high initial activity decreases moderately in the first 400 min, by ca. 15%, followed by a rather slow deactivation in the next 4000 min, until reaching a steady-state situation with a TOF of 3.0 s^{-1} after 5000–6000 min time on stream (with a total deactivation of ca. 26%). The activity and deactivation with time on stream agree well with those of comparable oxidatively pretreated Au/TiO_2 catalysts [45,52–54], though the extent of deactivation may differ for different catalysts and depending on the reaction conditions (see also Table S2 in the Supporting Information). It is generally accepted that the deactivation mainly results from the formation and accumulation of reaction inhibiting surface carbonate species on the catalyst surface

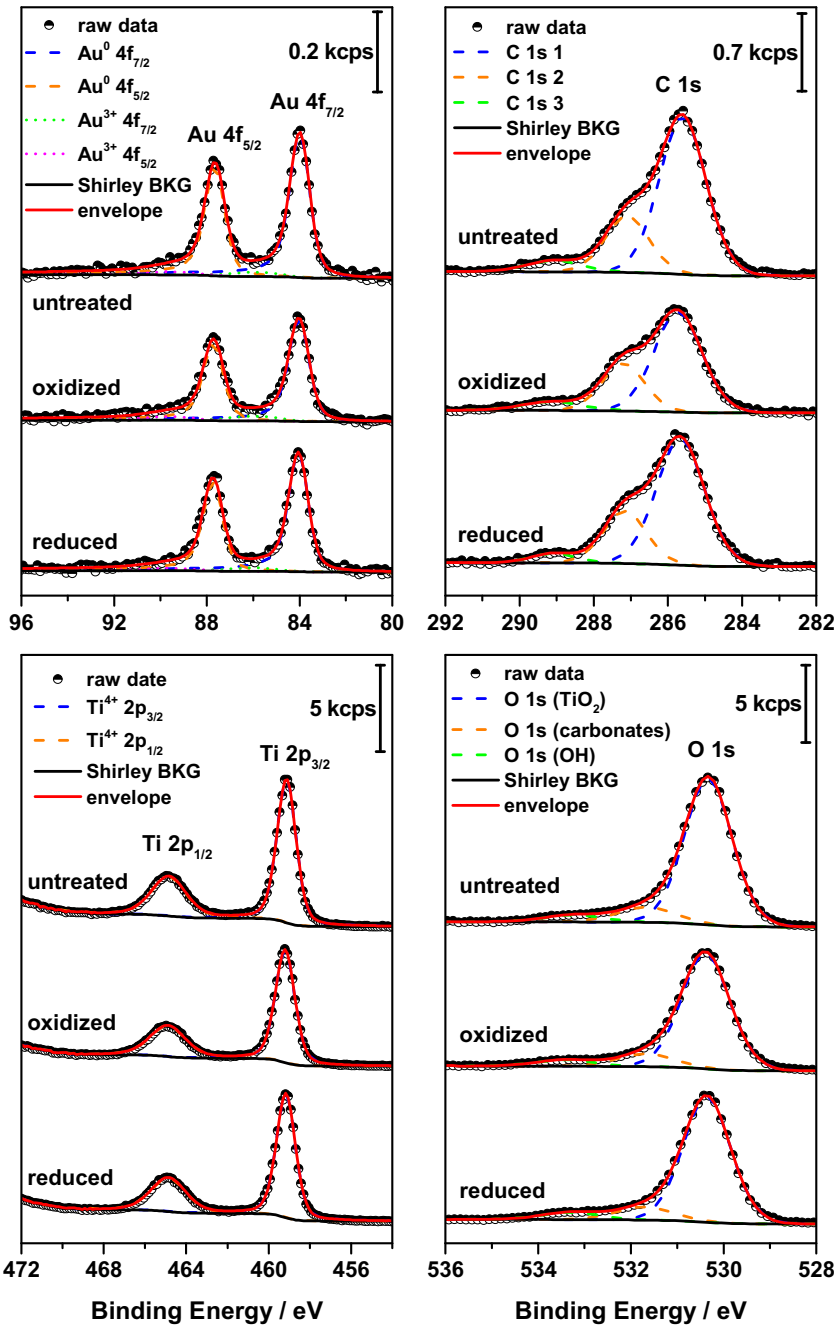

Fig. 2. XP spectra of the Au 4f, C 1s, Ti 2p, and O 1s signals obtained on Au/TiO_2 catalysts as received (untreated) and after oxidizing (O400, 10% O_2/90% N_2) or reducing (CO400, 10% CO/90% N_2) pretreatment.

rather than from sintering of Au NPs under present reaction conditions [45,53,54].

For the sample after CO400 pretreatment, in contrast, the activity is initially rather low and steadily increases with time on stream. This increase resembles an activation process, which results in an about twofold higher TOF after 6000 min reaction as compared to the initial activity (2.9 s^{-1} and 1.7 s^{-1}, respectively). Such an activation period during the CO oxidation on supported Au catalysts has rarely been reported, most probably due to the fact that most studies used oxidizing pretreatment procedures. Therefore we repeated the kinetic measurement after CO400 pretreatment several times under identical reaction conditions, always starting with a freshly pretreated catalyst, which confirmed the trends discussed above. The absolute activity, however, varied by about 40% between individual measurements (see Supporting Information, Fig. S2). Possible reasons for these discrepancies are discussed below and in the Supporting Information. Apart from these deviations in the absolute rates, the general trend of an initially low CO oxidation activity directly after CO400 pretreatment and its slow increase with time on stream during the following 1000 min reaction (and longer) is fully reproducible.

A similar catalytic behavior with an initial increase of the CO oxidation activity has already been reported before for reaction at 25 °C by Cunningham et al. (1% CO in air) and by Gupta et al. (10% CO, 5% O_2, rest He) for a vacuum annealed Au/TiO_2 catalyst and for a previously reduced Au/Fe_2O_3 catalyst, respectively [55,56]. In both studies the activity for CO oxidation was rather low in the reduced form of the catalysts, right after the formation

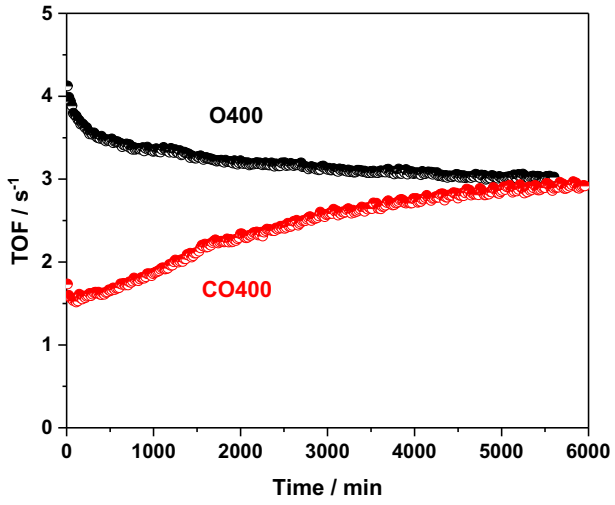

Fig. 3. Turn over frequencies (TOFs) for CO oxidation (1% CO, 1% O_2, 98% N_2) on Au/TiO_2 at 80 °C after *in situ* pretreatment at 400 °C in oxidizing (O400: 10% O_2/90% N_2) or reducing (CO400: 10% CO/90% N_2) atmosphere.

of defects in the support material (either due to vacuum annealing at elevated temperature or due to pretreatment in H_2), and increased with time on stream. The time dependence of the increase in CO oxidation activity with TOS of these two catalysts differed, however, significantly: while a continuous increase in activity was observed even after 150 h reaction on the Au/TiO_2 catalyst, the activity of Au/Fe_2O_3 reached steady-state already after 100 min. Nevertheless, the above authors consistently assigned this behavior to changes in the oxidation state of the support material, which is re-oxidized during the reaction due to the presence of O_2 in the reaction atmosphere [55,56]. It should be noted here that the authors did not distinguish between bulk and surface vacancies. In contrast, as discussed previously [15], we concluded based on indirect evidence that the lower CO oxidation activity directly after CO400 originates from the presence of TiO_2 bulk defects, which result in a modification of the electronic properties of the Au NPs due to electronic metal-support interactions (EMSIs) [15]. This was supported by a reaction measurement at 120 °C, where the activity of the CO400 pretreated catalyst was found to return much faster than at 80 °C to the same final activity as obtained for an O400 catalyst, as would be expected for a process limited by bulk oxygen vacancy diffusion. Returning to the present data, variations in the Au particle size, size distribution and particle shapes can be excluded as main reason for the differences in the initial activity and the temporal evolution of the reaction rates after pretreatment by O400 and CO400. As described above (Fig. 1), there are essentially no differences in the Au particle sizes or in the Au particle shapes for the differently pretreated samples, neither in the initial nor in the final period of the reaction.

To obtain more information on the physical origin of the lower activity of the reduced catalysts we monitored the evolution of surface species on Au/TiO_2 during CO oxidation and during CO adsorption, in the absence of O_2 in the reaction gas, after oxidizing and reducing pretreatment by *in situ* IR spectroscopy (DRIFTS) measurements. Spectra recorded during CO oxidation are presented in Fig. 4, while CO adsorption in the absence of O_2 is shown Fig. 5. We had already shown previously that adsorbed CO gives rise to slightly asymmetric peaks with their maximum at 2119 cm^{-1} (O400) and 2116–2119 cm^{-1} (CO400), where in the former case the intensity hardly varied with time, while in the latter case it initially started with a rather low intensity but slowly increased and slightly blue-shifted with time on stream. In the

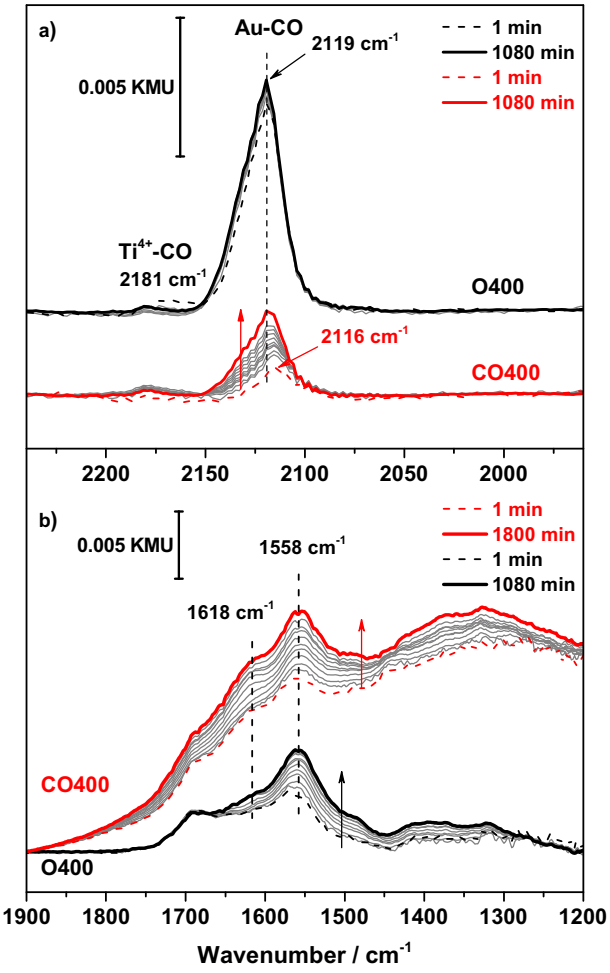

Fig. 4. Sequence of DRIFT spectra representing (a) the adsorbed CO species, and (b) the build-up of surface carbonate-like species, recorded during CO oxidation (1% CO, 1% O_2, 98% N_2) at 80 °C on a Au/TiO_2 catalyst pretreated at 400 °C in oxidizing (O400, 10% O_2/90% N_2) or reducing (CO400, 10% CO/90% N_2) atmospheres.

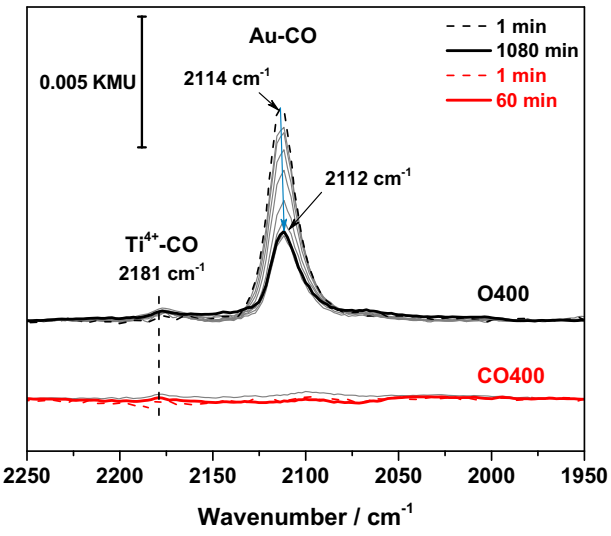

Fig. 5. Sequence of DRIFT spectra in the CO_{ad} region, recorded during CO adsorption (1% CO, 99% N_2) at 80 °C on a Au/TiO_2 catalyst, pretreated at 400 °C in oxidizing (O400, 10% O_2/90% N_2) or reducing (CO400, 10% CO/90% N_2) atmospheres.

CO adsorption experiments, in the absence of O_2, the differences are even more pronounced, since for the CO400 pretreated catalyst there was no indication for adsorbed CO, while for the O400 catalyst the CO_{ad} related peak decreases in intensity with time on stream, and red-shifts from 2114 to 2112 cm^{-1}.

We attribute the lower CO_{ad} coverage on the reductively pretreated catalyst under present reaction/adsorption conditions, reaching up to the complete absence of measurable CO adsorption, to a lower CO adsorption energy in the presence of TiO_2 bulk defects, which is at least partly responsible also for the lower CO oxidation activity of these catalysts (see also [15]). This would explain also the decrease in CO_{ad} band intensity during CO adsorption on the O400 pretreated sample, which is due to the creation of surface or surface near defects during exposure to CO. Unfortunately it was not possible to obtain detailed information on the electronic properties of the Au NPs at 80 °C directly after CO400 pretreatment, which in principle can be derived from the position of the absorption band of CO_{ad} on the Au NPs by CO adsorption measurements, since CO adsorption on the CO400 pretreated catalyst was below detection under these conditions. This is different for reaction at −20 °C, where CO_{ad} coverages on the Au NPs are much higher due to the slower CO desorption. Therefore, physical effects responsible for the lower CO_{ad} coverage/lower activity of the CO400 pretreated catalyst will be discussed in more detail in Section 3.3.

Similar to the kinetic experiments, also the DRIFTS measurements on CO400 pretreated samples were repeated several times to confirm these astonishing findings, and also in order to find possible explanations for the variations in the absolute rates observed in the initial period of the reaction in the kinetic measurements (see Fig. S2). These measurements revealed that the CO_{ad} coverage on the Au NPs is always lower than that on an O400 pretreated catalyst, but with some scatter in the extent, which seems to correlate with their variation in activity (see Fig. S3). Most likely, the absolute amount of bulk defect formation during the CO400 reducing pretreatment is not that well reproducible, leading to differences in the CO_{ad} coverage/adsorption strength and consequently in the activity.

Spectra recorded during reaction at 80 °C clearly indicate the build-up of carbonate-like surface species during CO oxidation. Interestingly, the type and the amount of surface carbonate species are almost identical for the differently pretreated catalysts (see Fig. 4). In both cases, significant amounts of carbonate-like species are formed right in the beginning of the CO oxidation reaction, within the first 1 min after introduction of the reaction gas mixture. The most prominent absorption bands were detected at 1618 cm^{-1} and 1558 cm^{-1}, which have been assigned to the ν_δ(OH) bending mode of adsorbed water and the ν_s(CO) stretching vibration of bidentate carbonates [53,57–60]. After both pretreatments the coverage of these species steadily increases with TOS. It is widely accepted that the formation and accumulation of surface carbonate species, most probably located on the support material and in part also at the Au-TiO_2 interface, is responsible for the deactivation of Au/TiO_2 catalysts during CO oxidation, as evidenced by several *in situ* IR spectroscopy studies [45,53,61–63]. From the comparison of their absorption intensities and the very similar temporal evolution after both pretreatments we conclude that the reducing pretreatment in CO/N_2, and thus the presence of bulk defects in TiO_2 has no distinct impact on the formation of these surface carbonate species. Accordingly, also for the CO400 catalyst a deactivation with time on stream would have been expected, similar to the decreasing activity observed after pretreatment in O_2/N_2 (see Fig. 3). This deactivation is, however, superimposed by the increasing activity with TOS due to the replenishment of bulk oxygen vacancies during reaction. Once all these vacancies are replenished, and the catalyst is fully oxidized again (after about 6000 min reaction), a steady-state situation with an almost identical activity compared to that after O400 is obtained. Considering that this represents the deactivated state of the Au/TiO_2 catalyst, it is obvious that also the catalyst sample after CO400 experienced a similar deactivation behavior, although this is not observed in kinetic measurements due to the more pronounced activation effects by the replenishment of bulk oxygen vacancies in the TiO_2 support.

3.2.2. *In situ* electrical conductivity measurements

The measurements presented so far did not provide direct experimental proof for the higher amount of TiO_2 bulk defects in Au/TiO_2 after CO400 pretreatment and their variation during subsequent reaction. Thus, our previous conclusions were based on logical consequences like the differences in the reaction characteristics and their changes with varying O_2 partial pressure or varying reaction temperature [15]. Using electron paramagnetic resonance (EPR) measurements, we had shown recently that exposing a Au/TiO_2 catalyst to CO at 120 °C for 10 min results in reactive removal of surface lattice oxygen and hence in the formation of surface lattice oxygen vacancies, but there are no data on the formation of bulk lattice defects [32]. To unambiguously demonstrate that there is indeed a higher amount of bulk defects after reducing pretreatment at elevated temperature (CO400), we additionally also measured the electrical conductivity directly after both pretreatments. These measurements were performed by the contact-free microwave cavity perturbation technique, which allows us to determine the conductivity *in situ* in a non-contact mode [34,35]. This conductivity is measured as a bulk property since the microwaves pervade the complete sample [34,64,65]. Assuming an essentially constant mobility of the charge carriers, changes in the conductivity provide information on changes in the amount of those charge carriers. The results of these measurements are summarized in Figs. 6 and 7. The microwave conductivities before, during, and after both pretreatments are illustrated in Fig. 6, and variations during subsequent CO oxidation (6 h) are shown in Fig. 7. Starting with the drying procedure, while keeping the catalyst in N_2 at 100 °C, there are essentially no differences between both samples, and the microwave conductivities are rather similar (1.8×10^{-3} S cm^{-1} and 0.7×10^{-3} S cm^{-1}) before CO400 and O400 pretreatment, respectively.

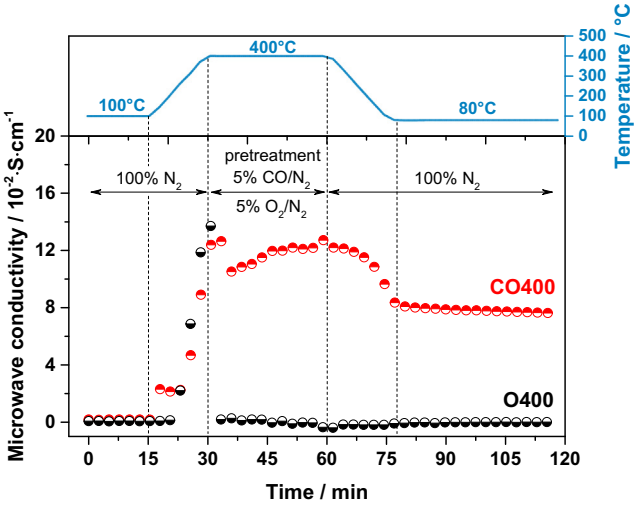

Fig. 6. Microwave conductivity of Au/TiO_2 before, during and after pretreatment at 400 °C in oxidizing (O400: 5% O_2/95% N_2) or reducing (CO400: 5% CO/95% N_2) atmosphere.

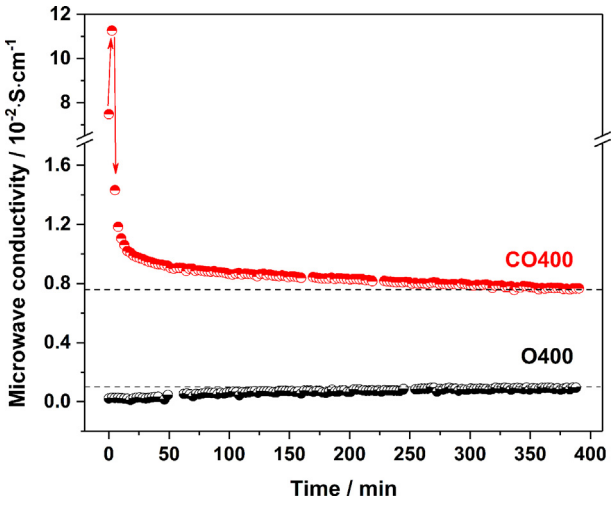

Fig. 7. Microwave conductivity of Au/TiO_2 during the CO oxidation (1% CO, 1% O_2, 98% N_2) at 80 °C after pretreatment in oxidizing (O400: 5% O_2/95% N_2) or reducing (CO400: 5% CO/95% N_2) atmosphere, respectively.

In the drying procedure the Au/TiO_2 catalyst is expected to be fully oxidized, with no or almost no bulk and surface defects [66]. During the following heating process to the temperature used for pretreatment (400 °C) in N_2, there is a sharp increase in the electrical conductivity up to about 0.13 S cm^{-1} for both samples. This increase in conductivity may (in part) be simply explained by the temperature increase, considering that semiconductors in general show an increasing conductivity with temperature. Another contribution may come from the desorption of adsorbed water/hydroxyl groups involving lattice oxygen during the heating procedure. Such species are still present on the catalyst surface at the beginning of the heating process (despite the previous drying procedure). This desorption results in the formation of surface oxygen vacancies, which finally leads to the observed increase in the microwave conductivity. Subsequently, for the Au/TiO_2 catalyst exposed to an oxidizing atmosphere during pretreatment, the conductivity decreases immediately once the catalyst is exposed to O_2/N_2 and, hence, re-oxidized. The conductivity is close to zero within several minutes in O_2/N_2 atmosphere, even at 400 °C (2.1×10^{-3} S cm^{-1}, see Fig. 6). During exposure to CO/N_2, in contrast, the microwave conductivity is about 0.12 S cm^{-1} during the whole period of the pretreatment, and decreases only by about 30% once the catalyst is cooled down to reaction temperature (80 °C) in a flow of pure N_2. At the end of the pretreatment procedure, which represents the starting point for the subsequent CO oxidation, the electrical conductivity after CO400 is 7.6×10^{-2} S cm^{-1}, and thus more than two orders of magnitude higher compared to the Au/TiO_2 catalyst after O400 (0.02×10^{-2} S cm^{-1}). Assuming again a constant (negligible changes) charge carrier mobility, this higher conductivity goes along with a significantly higher number of charge carriers, confirming that oxygen bulk defects in TiO_2 are indeed formed during CO400, but not during O400.

Upon switching from N_2 to reaction atmosphere (1% CO, 1% O_2, balance N_2), there are almost no changes for the Au/TiO_2 catalyst pretreated in oxygen (O400), except for a continuous, slight increase in conductivity to about 0.09×10^{-2} S cm^{-1} after 6 h CO oxidation (Fig. 7).

For the CO400 pretreated sample, in contrast, the conductivity decreases with time on stream, namely from 7.6×10^{-2} S cm^{-1} to 0.8×10^{-2} S cm^{-1}. The decay is very rapid in the initial phase of the reaction, as soon as the catalyst is exposed to the reaction atmosphere. (Note that there is also one data point with an even higher conductivity of about 11×10^{-2} S cm^{-1} for the sample pretreated in CO400 (see Fig. 7). We consider this, however, to be an artifact, probably due to changes in the reaction atmosphere composition.) Considering that the initial decrease in conductivity takes less than 3 min, we relate the rather fast decrease in conductivity to the replenishment of TiO_2 surface and surface near defects by O_2 from the gas phase, which is a rather fast process and is thus expected to occur on the timescale of seconds (see above and Refs. [15,18]). Even after this sharp decrease, however, the microwave conductivity on the CO400 pretreated catalyst sample is still a factor of about 70 higher than that after O400 pretreatment at the same reaction time. Moreover, as expected for a slow replenishment of bulk defects (on the time scale of minutes and hours, due to the slow oxygen diffusion in bulk TiO_2 under present reaction conditions) [67,68], there is only a very slow decrease in conductivity within the next 6 h time on stream. At that point the conductivity is 0.8×10^{-2} S cm^{-1}, and thus still about 10 times higher compared to that of the oxidatively pretreated sample after 6 h CO oxidation (see Fig. 7). This is in agreement with the findings from kinetic measurements performed under identical reaction conditions described above (see Fig. 3), in which the activities of the two samples are clearly different after 6 h on stream and only approach similar values after 100 h on stream.

Overall, these results on the electrical conductivity, which is related to changes in the number of charge carriers present in the Au/TiO_2 catalyst, in particular surface and bulk oxygen vacancies in TiO_2, clearly demonstrate that such defect sites are formed during pretreatment in CO/N_2 (CO400). Moreover, a significant number of those defect sites is still present during the subsequent CO oxidation reaction and are replenished only slowly. Considering that both, CO oxidation activity and CO adsorption strength on the Au NPs are lowered after CO400, and only increase slowly with time on stream (see Fig. 3), these findings clearly confirm our earlier proposal that the latter changes are related to the presence of TiO_2 bulk defects and changes therein [15].

3.3. Influence of TiO_2 bulk defects on the catalytic performance at −20 °C

In previous studies we had demonstrated that the dominant reaction pathway for CO oxidation on Au/TiO_2 catalysts changes with reaction temperature, and is different for reaction in the temperature regimes below or above about 0 °C, respectively [32]. From several experimental and theoretical studies there is convincing evidence that for room temperature and higher a Au-assisted Mars-van Krevelen mechanism dominates the overall reaction [18,22,24]. In this mechanism, TiO_2 surface lattice oxygen at the perimeter of the Au-TiO_2 interface represents the active oxygen species for CO oxidation, which is continuously removed and replenished upon interaction with CO and O_2, respectively. For reaction at lower temperatures, however, the removal of TiO_2 surface lattice oxygen by CO is strongly inhibited, indicating that this surface reaction is an activated process. This was explicitly demonstrated by the strongly reduced or even completely inhibited removal of TiO_2 surface lattice oxygen in Au/TiO_2 catalysts upon reaction with CO, and thus an inhibited TiO_2 surface reduction at reaction temperatures of −20 °C and −90 °C [32]. We tentatively suggest that under these conditions, in the range of low temperatures, the mechanism proposed by Green et al., involving the formation of a molecular adsorbed [CO···O_2] intermediate at the perimeter sites and their subsequent reactive decomposition to CO_2 and O_{ad}, becomes increasingly dominant [69]. It should also be noted that under these conditions, the continuous reaction on Au/TiO_2 is strongly hindered by adsorption of product CO_2, which strongly interacts with the Au/TiO_2 catalyst, resulting in a self-poisoning effect [70]. We therefore proposed that the desorption

of $CO_{2,ad}$ is the rate limiting step for CO oxidation on Au/TiO_2 at reaction temperatures below −20 °C. Finally, the much lower activity of Au/TiO_2 compared to $Au/Mg(OH)_2$ at reaction temperatures below 0 °C, which is in complete contrast to their behavior above room temperature, lead us to the conclusion that there is a change of support effects with temperature [70].

Accordingly, the influence of TiO_2 bulk defects on the catalytic performance may also be fundamentally different at lower reaction temperatures. For that reason, we next measured and compared the CO oxidation activity of Au/TiO_2 at −20 °C (Section 3.3.1) after pretreatment in oxidizing (O400) and reducing (CO400) atmosphere, and complemented this by *in situ* IR spectroscopy (DRIFTS) measurements under identical reaction conditions (Section 3.3.2).

3.3.1. CO oxidation activity at −20 °C

Fig. 8 illustrates the temporal evolution of the catalytic activity on the differently pretreated Au/TiO_2 catalysts for CO oxidation at a reaction temperature of −20 °C. Unlike the catalytic behavior at 80 °C, the initial activity of the catalyst after CO400 pretreatment at −20 °C is significantly higher compared to that after O400 pretreatment (TOF values of 0.22 s^{-1} and 0.12 s^{-1}, respectively). Hence, in this case TiO_2 bulk defects have a positive influence on the catalytic activity, contrasting the behavior for reaction at 80 °C. Moreover, also the temporal evolution of the activity at −20 °C after CO400 is completely different from that at 80 °C after the same pretreatment. Instead of an activation with TOS we here observe a continuous decrease in activity, as it has been observed after oxidizing pretreatment (O400) at 80 °C. This deactivation continues for at least 1000 min, and results in a steady-state TOF value of 0.12 s^{-1}. The same reaction behavior is observed for the Au/TiO_2 catalyst pretreated in oxygen, which also shows a continuous decrease in activity with time on stream at −20 °C, and even an almost identical extent of deactivation throughout the reaction (57% deactivation, see Fig. 8b). The resulting reaction rates (in TOFs) after 1000 min CO oxidation are 0.05 s^{-1} for the O400 catalyst (initial value 0.12 s^{-1}) and 0.12 s^{-1} for the CO400 catalyst (initial value 0.22 s^{-1}), respectively. The fact that both samples end up with a relative activity of 43% compared to its highest (initial) activity, points to a similar mechanism for the catalyst deactivation under these conditions (see also our discussion on deactivation at 80 °C above). This will be discussed in more detail below (Section 3.3.2).

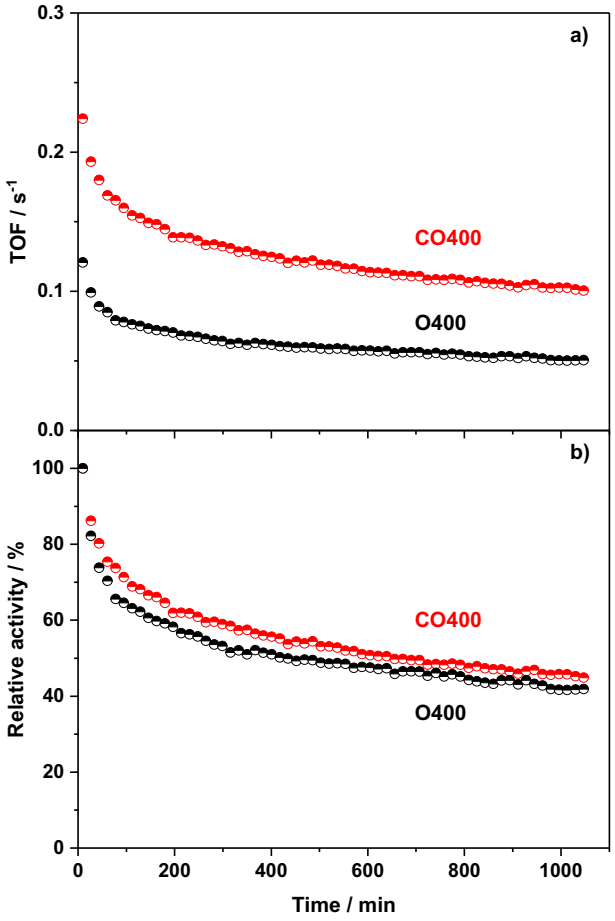

Fig. 8. (a) Turn over frequencies (TOFs) and (b) relative activities during the CO oxidation (1% CO, 1% O_2, 98% N_2) at −20 °C on Au/TiO_2 after *in situ* pretreatment at 400 °C in oxidizing (black: O400, 10% O_2/90% N_2) or reducing (red: CO400, 10% CO/90% N_2) atmosphere.

Following our above line of arguments, where we assigned the differences in activity at 80 °C after the two pretreatments to the absence/presence of TiO_2 bulk defects, we expect that the higher activity after CO400 at −20 °C also originates from the formation of such defects during pretreatment. In this case, however, they have a positive impact on the catalytic activity. Furthermore, it is plausible to conclude that at −20 °C oxygen bulk diffusion in TiO_2 is strongly hindered and, hence, even slower compared to that at a reaction temperature of 80 °C, for which it took already about 6000 min until the catalyst reached its fully oxidized state again (see above, Fig. 3). For that reason, one would expect that at −20 °C the catalyst maintains its strongly reduced state throughout the 1000 min reaction. This fits well to our observation that the differences in activity after both pretreatments do not get smaller during the CO oxidation reaction, but stay essentially constant.

It is also interesting to note that, different from the present findings for the STREM Au/TiO_2 catalyst, we observed no deactivation at all for CO oxidation at −20 °C on a similarly prepared, homemade Au/TiO_2 catalyst under the same reaction conditions [70], although both catalysts were prepared by deposition precipitation, with a similar mean Au particle size of ca. 2.5 nm, but differed in Au loading and pretreatment.

3.3.2. Formation of surface species during reaction at −20 °C

More insight into modifications of the catalyst surface during reaction is gained from *in situ* IR measurements, which may also provide further information on the origin of the beneficial effect of bulk defects on the CO oxidation activity of Au/TiO_2 at −20 °C. First, we will focus on the temporal evolution of the CO_2 band on the two differently pretreated catalysts during CO oxidation at −20 °C, which is illustrated in Fig. 9a. In contrast to the IR spectra recorded during CO oxidation at room temperature and higher, e.g., at 80 °C [53], we did not observe the typical feature of gas phase CO_2, which is characterized by its P- and R-branch and originates from the simultaneous vibrational and rotational excitation of the CO_2 molecule. Instead, for reaction at −20 °C we mainly find adsorbed CO_2 product species, which are characterized by a single IR absorption band at 2347 cm^{-1}, for which rotation is strongly hindered. This fully agrees with our recent findings, where we demonstrated the presence of $CO_{2,ad}$/absence of $CO_{2,g}$ on a similar type Au/TiO_2 catalyst at this low temperature [70]. Note that according to the kinetic measurements also $CO_{2,g}$ is formed during the reaction, but its rather low concentration (ca. 200 ppm, calculated from the kinetic measurement) would result in a very weak $CO_{2,g}$ IR doublet signal, which is buried beneath the intense $CO_{2,ad}$ band and can be hardly resolved by DRIFTS measurements.

Similar to the activities, the coverage of adsorbed $CO_{2,ad}$ species (based on the absorption band intensity) is about two times higher on the CO400 pretreated sample than on the O400 pretreated sample. Furthermore, for both catalysts the $CO_{2,ad}$ band intensity

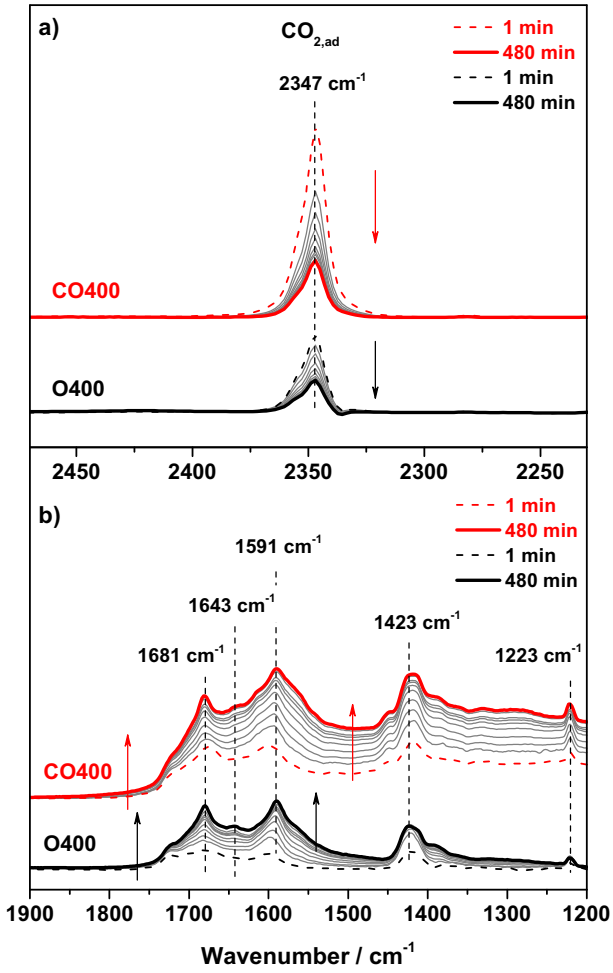

Fig. 9. Sequence of DRIFT spectra illustrating the evolution of (a) CO_2 and (b) carbonate surface species during the CO oxidation reaction (1% CO, 1% O_2, 98% N_2) at −20 °C on Au/TiO_2 catalyst pretreated at 400 °C in oxidizing (black: O400, 10% O_2/90% N_2) or reducing (red: CO400, 10% CO/90% N_2) atmosphere, respectively.

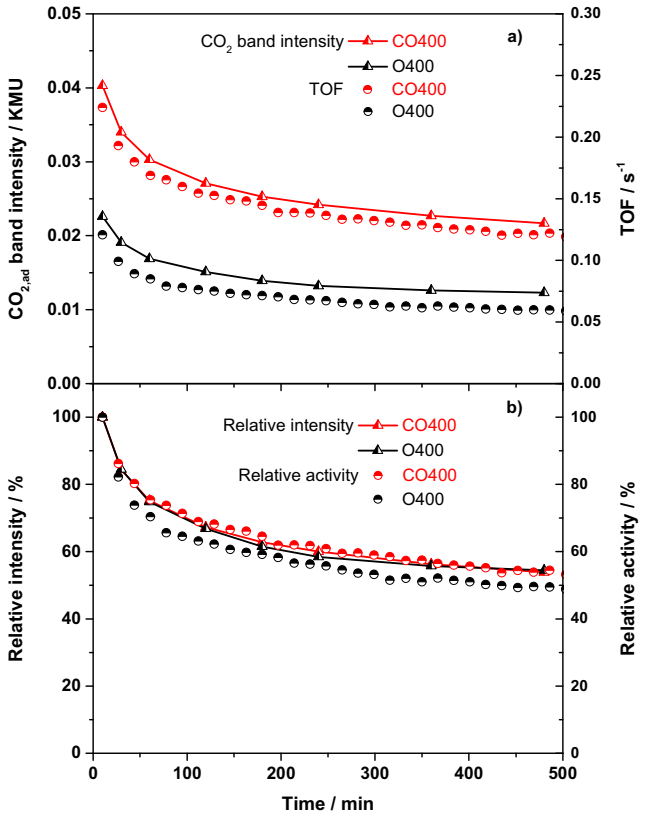

Fig. 10. Temporal evolution of the integrated total (a) and relative (b) IR band intensities of $CO_{2,ad}$ as well as the absolute and relative CO_2 formation rates (from Fig. 8) during the CO oxidation reaction (1% CO, 1% O_2, 98% N_2) at −20 °C on Au/TiO_2 catalyst pretreated at 400 °C in oxidizing (black: O400, 10% O_2/90% N_2) or reducing (red: CO400, 10% CO/90% N_2) atmosphere, respectively.

decreases with TOS at a similar pace relative to their initial (maximum) coverage in the beginning of the reaction. Overall, there is a rather good correlation between the time dependence of the CO_2 band intensity and the catalytic activity determined in the kinetic measurements (see Fig. 10). We could show recently [70] for a similar type Au/TiO_2 catalyst that the desorption of $CO_{2,ad}$ from the TiO_2 support is rather slow and appears to be the rate-limiting step for the catalytic CO oxidation below 0 °C. A similar proposal was put forward also by Chang et al. [71]. Based on the close relation between the coverage of adsorbed CO_2 species and activity for continuous $CO_{2,g}$ formation this seems to hold true also for the present case, for reaction on both the O400 and the CO400 catalyst at −20 °C.

To verify that fundamental aspects of the reaction and deactivation behavior of the two catalysts are identical for reaction at −20 °C, with the CO400 catalyst only being more active, we performed CO_2 desorption experiments on the differently pretreated STREM Au/TiO_2 catalysts, using the same procedure as described previously [70]. After running the CO oxidation reaction at −20 °C for 120 min, the reaction gas was switched from CO/O_2/N_2 to a gas stream containing N_2 only, keeping the catalyst at a constant temperature of −20 °C in order to follow the isothermal desorption of CO_2 (see Supporting information, Fig. S4). For the O400 pretreated catalyst, 74% of the $CO_{2,ad}$ band intensity was lost after 10 min TOS of N_2 purging, and rather similar results were obtained also for the CO400 pretreated STREM Au/TiO_2 catalyst. Apparently, the presence of TiO_2 bulk defects has no measurable impact on the interaction between CO_2 and the catalyst surface, confirming our conclusions derived from the similar reaction and deactivation behavior.

DRIFT spectra illustrating the build-up of surface carbonate species on the two differently pretreated catalysts during the CO oxidation reaction at −20 °C are shown in Fig. 9b. In general, the coverages of surface carbonate species increase with time on stream on both samples during reaction. Furthermore, both the types as well as the amount of surface carbonate species formed on the two samples seem to be identical. Hence, similar to the observation at 80 °C (see Fig. 4), also at −20 °C the presence of bulk defects seems to have no influence on the formation of surface carbonate species during CO oxidation. Note that in addition to the bands observed for reaction at 80 °C, several new bands were observed here. Following the assignments in previous IR studies [58–60,72,73], we associate the additional bands at 1643 cm^{-1}, 1423 cm^{-1} and 1223 cm^{-1} to bicarbonate species, and the bands at 1681 cm^{-1} and 1591 cm^{-1} to bridged and bidentate carbonates. The main findings from Fig. 9 are as follows: while the build-up of surface bicarbonate species stops in the early stages of the reaction, after ca. 10 min to 30 min on stream, the coverage of the two types of carbonates continuously increases with TOS. Specifically, the amount of bidentate carbonates increases significantly on both the CO400 and the O400 pretreated samples with time on stream, by ca. 40% from 10 min to 120 min (see Fig. S5), which agrees well with the ca. 30–40% deactivation of the catalyst determined in kinetic measurements in the same time span under these

conditions (see Fig. 8). From 120 min to 480 min, the coverage of bidentate carbonates slowly increases by another 20%, which again fits to the slower deactivation of the catalyst in this time range (see Fig. S5). Therefore, we tentatively propose that in addition to self-poisoning by adsorbed CO_2, also for reaction at −20 °C the build-up of bidentate carbonate species contributes to the deactivation of the catalyst, blocking either directly the active sites or the diffusion of active CO or O_2 species to these active sites.

Finally, we investigated the influence of bulk defects on the electronic/chemical properties of the Au NPs using adsorbed CO as probe molecule in the presence (reaction condition) and absence (CO titration) of O_2 at −20 °C (see Fig. 11). As mentioned above, this refers particularly to the questions of whether there is evidence for (i) a reduced accessibility of the Au NP surface, e.g., due to partial overgrowth by TiO_x on the CO400 pretreated sample, and for (ii) differences in the Au-CO interactions. The latter would be indicated by differences in the adsorption strength and by shifts in the CO vibrational band. For adsorption/reaction at 80 °C this information was available only to a limited extent, since measurable CO adsorption on the CO400 pretreated Au/TiO_2 catalyst was only observed after partial re-oxidation, during the CO oxidation reaction [15]. Exposure of the O400 pretreated sample to a reaction gas mixture at −20 °C yields a sharp band at 2181 cm^{-1} which is associated with CO adsorbed on coordinatively unsaturated Ti^{4+} site [41,69], and a broad signal with a pronounced maximum and a shoulder on its higher frequency side in the Au-CO_{ad} region, in the range between 2150 and 2075 cm^{-1}. Here two bands can be resolved after peak deconvolution using Lorentz functions (see Fig. S6), which are positioned at 2109 cm^{-1} and 2124 cm^{-1}, respectively. The band at 2109 cm^{-1} is generally assigned to CO adsorbed on metallic Au (denoted as Au^0) [42], the higher wavenumber signal (2124 cm^{-1}) was attributed to CO adsorbed on electron-deficient/positively charged $Au^{\delta+}$-CO sites [42]. Those latter sites may either be located at the perimeter of the Au-TiO_2 interface (perimeter sites) involving Au-O-Ti bonds [74–76], or they may be related to co-adsorption of oxygen species [41]. Except for a very small increase of the intensity of this band in the first 10 min of the reaction, the intensity of all three bands in the CO_{ad} region remained essentially constant during the whole time of the reaction, from 1 min to 480 min TOS. It is worth to note that the CO_{ad} band at 2124 cm^{-1} was not observed during CO adsorption/CO oxidation at 80 °C. Most simply, this may be due to a too low steady-state CO_{ad} coverage on these sites at 80 °C under these conditions. The appearance of this $Au^{\delta+}$-CO band under reaction conditions at −20 °C indicates a higher local coverage of CO molecules on these sites.

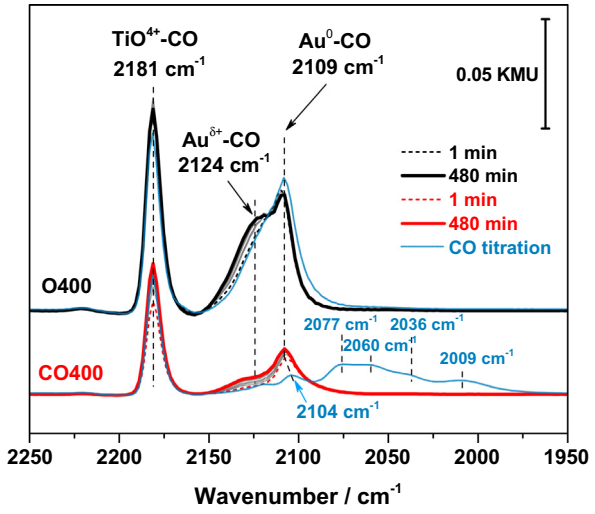

Fig. 11. Sequence of DRIFT spectra representing adsorbed CO species (CO_{ad}), recorded during CO oxidation (1% CO, 1% O_2, 98% N_2) and CO adsorption (1% CO, 99% N_2, recorded after 10 min) at −20 °C on Au/TiO_2 catalysts pretreated at 400 °C in oxidizing (O400, 10% O_2/90% N_2) or reducing (CO400, 10% CO/90% N_2) atmosphere. Note that the gas phase CO signal is already subtracted.

In the CO adsorption measurement on the O400 pretreated Au/TiO_2 catalyst, during catalyst exposure to 1% CO/N_2 at −20 °C, the spectrum shows a much less pronounced shoulder at 2124 cm^{-1} (see the blue spectrum in Fig. 11). Obviously, the $Au^{\delta+}$-CO sites are much less populated under these conditions. After peak deconvolution (see Fig. S6), one can still resolve a contribution from this band, but it is much smaller than during reaction. Based on the lower intensity of this band in the absence of O_2 it is most probably at least partly due to coadsorbed oxygen, though contributions from perimeter sites, arising from a slight removal of surface lattice oxygen at the Au perimeter sites during CO adsorption at −20 °C, cannot be fully excluded.

Similar but less intense CO_{ad} related bands were observed during CO oxidation at −20 °C on the CO400 pretreated sample. With time on stream, the coverage of both Au-CO_{ad} and Ti^{4+}-CO_{ad} increased slowly. Following the above line of arguments, this increase with time on stream can be attributed to a slow re-oxidation of the catalyst, which as expected for bulk vacancy re-oxidation is rather slow at this low temperature. For comparison we note that even for reaction at 80 °C complete re-oxidation of bulk defects takes about 100 h under present reaction conditions (see Fig. 3). In contrast, as we found recently, re-oxidation of surface oxygen vacancies by reaction with O_2 in the gas phase at −20 °C can occur very fast and essentially on the same time scale as re-oxidation at 80 °C.

Before discussing these results in more detail, we will first characterize CO adsorption at −20 °C on the CO400 pretreated catalyst. As shown in Fig. 11 (blue spectrum), the Au^0-CO band was red-shifted to 2104 cm^{-1}. In addition, a set of new bands in the lower frequency region from 2077 cm^{-1} to 2009 cm^{-1} was observed. According to earlier studies, these bands can be assigned to CO adsorbed on negatively charged Au species ($Au^{\delta-}$), which result from electron donation from the defect rich TiO_{2-x} support to the Au NPs [41–43,63,77–79]. It is important to note that these negatively charged $Au^{\delta-}$ species were neither detected for CO adsorption on the fully oxidized catalyst (O400 pretreated) at −20 °C, in the absence of O_2 in the gas phase, nor under reaction conditions, in the presence of O_2, independent of the pretreatment. This means, that these $Au^{\delta-}$ species cannot be (solely) related to bulk defects, but must require the presence of surface and near surface defects, which are rapidly re-oxidized upon interaction with the reaction gas mixture. On the other hand, we found that the $Au^{\delta-}$ species can also be formed on the fully oxidized catalyst at −20 °C, when the contact time of the catalyst with a CO atmosphere is sufficiently long, e.g., more than 60 min. Since bulk defect formation is essentially inhibited under these conditions, this means that these $Au^{\delta-}$ species result from charge transfer from surface defects or near surface defects, which can still be formed at a low rate at this temperature, as was demonstrated recently by EPR measurements [32]. Finally we would like to note that we observed the formation of a very weak band of adsorbed CO_2 during exposure to CO (see Fig. S7), which most likely is due to reaction either with surface lattice oxygen (see above) or with traces of O_2 in the reaction cell.

The above results first of all confirm the weaker bonding of CO to the Au NPs in the presence of bulk defects. Considering that significant amounts of CO can adsorb on the CO400 catalyst at −20 °C, while at 80 °C CO adsorption is essentially inhibited. The absence of CO adsorption at 80 °C cannot be solely explained by surface blocking, e.g., by overgrowth by a TiO_x layer. This must at least

partly be due to weaker CO_{ad} bonding on the Au NPs. This confirms our previous proposal that for the CO400 pretreated catalyst the interaction of CO with the Au NPs is strongly modified by electronic effects, by electronic metal-support interactions (EMSIs), induced by the presence of bulk defects [15]. Interestingly, the resulting shift in C-O frequency (for CO adsorption) is rather weak, from 2109 (O400) to 2104 cm^{-1} (CO400).

The presence of bulk defects seems to have much less impact on the CO adsorption and CO adsorption energy on the TiO_2 support, which is indicated by the comparable intensities of the Ti^{4+}-CO_{ad} bands on the samples after oxidizing and reducing pretreatment, respectively. This closely resembles our findings for CO_2 adsorption on the TiO_2 support, which was also little affected by the presence of bulk defects.

Finally, it should be noted that along with the $Au^{\delta-}$-CO_{ad} species, we also observed a tiny signal at 2124 cm^{-1} during the CO adsorption measurement at −20 °C. Since the co-existence of $Au^{\delta+}$ and $Au^{\delta-}$ species tends to be unlikely, the signal at 2124 cm^{-1} observed during CO titration on the pre-reduced catalyst could possibly be attributed to CO adsorbed on Ti^{3+} surface species, whose presence was indicated by previous IR [80–82] and EPR [32,83–85] measurements on reduced TiO_2.

Correlating the findings from the *in situ* IR measurements with the trends in the CO oxidation activity leads to the following results. First of all for reaction at 80 °C the presence of bulk defects is clearly related to a distinct lowering of the activity. This is at least partly caused by a lower CO_{ad} coverage on the Au NPs due to a lowering of the CO adsorption energy, which in turn is caused by a distinct modification of the electronic/chemical properties of the Au NPs due to electronic metal-support interactions caused by the bulk defects. Hence, the extensive data present here fully confirm our recent proposal [15].

Chen and Goodman had proposed that negatively charged Au species ($Au^{\delta-}$) are crucial for a high CO oxidation activity, specifically for the activation of O_2 by electron transfer forming superoxo-like species [28,86,87]. The results presented above clearly indicate that $Au^{\delta-}$-CO_{ad} species characterized by CO_{ad} bands in the range 2077 cm^{-1} and below are not present under reaction conditions, independent of the pretreatment, and that the presence of bulk defects results in a weaker CO bonding, going along with a lower CO oxidation activity at 80 °C.

Also for adsorption/reaction at −20 °C, the CO_{ad} coverage on the Au NPs is significantly lower on the CO400 than on the O400 pretreated catalyst. In this case, however, the electronic modification of the Au NPs due to the TiO_2 bulk defect induced EMSIs have a positive effect on the CO oxidation activity, in contrast to the behavior at 80 °C, where the effect was opposite. Partly this can be explained by the much lower effects of the CO_{ad} coverage under these conditions. Now also CO adsorption on Ti^{4+} sites is significant and has to be considered. At this temperature, CO_{ad} species are still considered to be mobile on the surface [69], populating different adsorption sites according to thermodynamic equilibrium. In that case, both Au-CO and Ti^{4+}-CO species can be considered as reservoir, which can reach the active sites such as perimeter sites and react to CO_2. Considering the much higher number of Ti^{4+} sites and the comparable population of these sites on both catalysts, the differences in total CO_{ad} coverage on the O400 and CO400 catalysts are much less pronounced for reaction at −20 °C than at 80 °C. In this case the effect of the lower CO adsorption strength on the Au NPs after CO400 pretreatment has much less impact on the reaction at low temperatures than at higher temperatures. This would not explain, however, a higher activity of the CO400 pretreated Au/TiO_2 catalyst compared to the O400 one. The latter requires a change in the rate limiting step or, more likely, in the dominant reaction mechanism for CO oxidation when going from 80 °C to −20 °C, in addition to the CO_{ad} coverage effects. This fits perfectly to our previous conclusion of a temperature dependent change in the dominant reaction pathway at temperatures in the range of 0 °C, from a Au-assisted Mars-van Krevelen mechanism above that level to a mechanism with a different type of oxygen activation, possibly by reaction between adsorbed O_2 and CO_{ad} at perimeter sites, as it had been shown by Green et al. for reaction at much lower temperatures, in the range of 110–130 K [69].

Overall, we expect that similar electronic interactions can at least in principle operate also on other Au catalysts supported on reducible oxides and also on other oxide supported noble metal catalysts, and also in other catalytic reactions. For more active noble metals it has to be considered however, that in most cases the reaction will proceed via a Langmuir-Hinshelwood mechanism, where, e.g., coverage effects may be more complicated. Furthermore, continuous effects during the reaction can only be expected if bulk vacancies persist during the reaction, which either requires very low reaction temperatures to kinetically block replenishment of bulk vacancies or, more realistically, reducing reaction conditions, as experienced, e.g., in hydrogenation reactions. This will be topic of future studies.

4. Conclusions

Aiming at a detailed understanding of the role of electronic metal-support interactions (EMSIs) in the CO oxidation reaction on metal oxide supported Au catalysts and its temperature dependence, we have investigated the interaction of CO and the CO oxidation with/on a Au/TiO_2 catalyst in the presence and absence of TiO_2 bulk oxygen vacancies at reaction temperatures of 80 °C and −20 °C. TiO_2 bulk defects were generated by pretreatment in strongly reducing atmosphere at elevated temperatures. The adsorption/reaction properties of these catalysts were compared with those of similar catalysts pretreated in an oxidizing atmosphere. Combining kinetic measurements with detailed catalyst characterizations, including *in situ* electrical conductivity and *in situ* DRIFTS measurements, we arrive at the following conclusions:

(i) Reducing pretreatment (CO400) leads to a distinct increase in electrical conductivity and, assuming about constant charge carrier mobilities, in the number of charge carriers, most probably TiO_2 bulk defects. The conductivity is stable in N_2 at 80 °C, while upon exposure to the reaction atmosphere at that temperature it first decreases rapidly, followed by a slow further decay. The initial rapid decay is associated with oxidation of surface vacancies, while the subsequent slow decay latter is attributed to the slow removal of charge carriers, i.e., defect sites, in the bulk of the TiO_2 support, which are only slowly oxidized under reaction conditions, despite the net oxidizing reaction atmosphere.

(ii) Electronic metal-support interactions (EMSIs) induced by the presence of TiO_2 bulk defects have a negative impact on the CO oxidation activity at 80 °C, which at least partly originates from a lower CO adsorption strength and hence drastically reduced steady-state CO_{ad} coverage on the electron rich Au NPs in the presence of bulk defects.

(iii) At an adsorption/reaction temperature of −20 °C, these EMSIs also lower the CO adsorption strength on the Au NPs. In contrast to reaction at 80 °C, however, they promote the CO oxidation reaction. We attribute this mainly to (a) a drastically increased coverage of mobile CO_{ad} species on the CO400 pretreated catalyst at low temperatures, particularly on the Ti^{4+} sites, which are less affected by TiO_2 bulk

defects than the Au NPs and (b) an enhanced activation of molecular oxygen due to the extra charges on the Au NPs resulting from EMSIs, most likely at the perimeter sites.

On the other hand, bulk defects have little effect (a) on the $CO_{2,ad}$ desorption rate from the support, which was proposed to be the rate limiting step for CO oxidation on Au/TiO_2 catalysts at low temperatures (≤ -20 °C), and (b) on the deactivation of the catalyst under these conditions. The latter was shown to result from the build-up of bidentate carbonate species during reaction, both at 80 °C and at −20 °C.

(iv) Finally, if surface defects are present as well, the negative charge on the Au NPs can be sufficient to result in a distinct red-shift of the CO_{ad} related band to wave numbers in the range of 2000–2077 cm^{-1}. In contrast to the slow removal of effects related to bulk defects, these bands and hence the increased negative charge on the Au NPs decay immediately in the presence of O_2 in the reaction gas, i.e., upon re-oxidation of (near) surface oxygen vacancies.

In summary, we could show that bulk defects have a distinct effect on the CO oxidation behavior of Au/TiO_2 catalysts, which may differ also depending on the temperature. Such kind of effects are proposed to be of general validity for Au catalysts supported on (bulk) reducible metal oxides. However, they will not be operative under 'normal' reaction conditions, for reaction above room temperature, in the presence of an oxidizing reaction atmosphere and after oxidizing pretreatment, because under these conditions the steady-state concentration of bulk oxygen vacancies is in most cases negligible.

Acknowledgement

We gratefully acknowledge Mr. S. Blessing (Ulm University), Mr. T. Buhle (Fritz-Haber Institute), and Dr. F. Girgsdies (Fritz-Haber Institute) for the XRD measurements.

Appendix A. Supplementary material

Supplementary data associated with this article can be found, in the online version, at http://dx.doi.org/10.1016/j.jcat.2017.07.029.

References

[1] S.J. Tauster, Acc. Chem. Res. 20 (1987) 389–394.
[2] A.T. Bell, Science 299 (2003) 1688–1691.
[3] Q. Fu, T. Wagner, Surf. Sci. Rep. 62 (2007) 431–498.
[4] J.A. Farmer, C.T. Campbell, Science 329 (2010) 933–936.
[5] A. Bruix, J.A. Rodriguez, P.J. Ramírez, S.D. Senanayake, J. Evans, J.B. Park, D. Stacchiola, P. Liu, J. Hrbek, F. Illas, J. Am. Chem. Soc. 134 (2012) 8968–8974.
[6] J.C. Matsubu, S. Zhang, L. DeRita, N.S. Marinkovic, J.G. Chen, G.W. Graham, X. Pan, P. Christopher, Nat. Chem. 9 (2017) 120–127.
[7] S.J. Tauster, S.C. Fung, R.L. Garten, J. Am. Chem. Soc. 100 (1978) 170–175.
[8] C.T. Campbell, Nat. Chem. 4 (2012) 597–598.
[9] X. Lin, B. Yang, H.-M. Benia, P. Myrach, M. Yulikov, A. Aumer, M.A. Brown, M. Sterrer, O. Bondaschurk, E. Kieseritzky, J. Rocker, T. Risse, H.-J. Gao, N. Nilius, H.-J. Freund, J. Am. Chem. Soc. 132 (2010) 7745–7749.
[10] Y. Cui, C. Stiehler, N. Nilius, H.J. Freund, Phys. Rev. B 92 (2015) 075444.
[11] H.J. Freund, J. Am. Chem. Soc. 138 (2016) 8985–8996.
[12] X. Shao, S. Prada, L. Giaordano, G. Pacchioni, N. Nilius, H.-J. Freund, Angew. Chem. Int. Ed. 50 (2011) 11525–11527.
[13] X. Shao, N. Nilius, H.J. Freund, J. Am. Chem. Soc. 134 (2012) 2532–2534.
[14] B. Yoon, H. Häkkinen, U. Landman, A.S. Wörz, M. Antonietti, S. Abbet, K. Judai, U. Heiz, Science 307 (2005) 403–407.
[15] Y. Wang, D. Widmann, R.J. Behm, ACS Catal. 7 (2017) 2339–2345.
[16] H. Iddir, S. Ögüt, N.D. Browning, M.M. Disko, Phys. Rev. B 72 (2005) 081407.
[17] H. Tang, J. Wei, F. Liu, B. Qiao, X. Pan, L. Li, J. Liu, J. Wang, T. Zhang, J. Am. Chem. Soc. 138 (2016) 56–59.
[18] D. Widmann, R.J. Behm, Angew. Chem. Int. Ed. 50 (2011) 10241–10245.
[19] D. Widmann, R.J. Behm, ACC Chem. Res. 47 (2014) 740–749.
[20] L. Li, A. Wang, B. Qiao, J. Lin, Y. Huang, X. Wang, T. Zhang, J. Catal. 299 (2013) 90–100.
[21] H.Y. Kim, G. Henkelman, J. Phys. Chem. Lett. 4 (2013) 216–221.
[22] M.A. Saqlain, A. Hussain, M. Siddiq, A.R. Ferreira, A.A. Leitao, Phys. Chem. Chem. Phys 17 (2015) 25403–25410.
[23] M. Lohrenscheit, C. Hess, ChemCatChem 8 (2016) 523–526.
[24] Y. Maeda, Y. Iizuka, M. Kohyama, J. Am. Chem. Soc. 135 (2013) 906–909.
[25] E. Wahlström, N. Lopez, R. Schaub, P. Thostrup, A. Rønnau, C. Africh, E. Laegsgaard, J.K. Nørskov, F. Besenbacher, Phys. Rev. Lett. 90 (2003) 026101.
[26] W.T. Wallace, B.K. Min, D.W. Goodman, J. Mol. Catal. A 228 (2005) 3–10.
[27] A.S. Wörz, U. Heiz, F. Cinquini, G. Pacchioni, J. Phys. Chem. B 109 (2005) 18418–18426.
[28] M. Chen, D.W. Goodman, Acc. Chem. Res. 39 (2006) 739–746.
[29] S. Laursen, S. Linic, J. Phys. Chem. C 113 (2009) 6689–6693.
[30] G. Pacchioni, Phys. Chem. Chem. Phys. 15 (2013) 1737–1757.
[31] D.W. Goodman, Catal. Lett. 99 (2005) 1–4.
[32] D. Widmann, A. Krautsieder, P. Walther, A. Brückner, R.J. Behm, ACS Catal. 6 (2016) 5005–5011.
[33] B. Schumacher, V. Plzak, J. Cai, R.J. Behm, Catal. Lett. 101 (2005) 215–224.
[34] M. Eichelbaum, M. Hävecker, C. Heine, A. Karpov, C.-K. Dobner, F. Rosowski, A. Trunschke, R. Schlögl, Angew. Chem. Int. Ed. 51 (2012) 6246–6250.
[35] M. Eichelbaum, R. Stößer, A. Karpov, C.-K. Dobner, F. Rosowski, A. Trunschke, R. Schlögl, Phys. Chem. Chem. Phys. 14 (2012) 1302–1312.
[36] C. Heine, M. Hävecker, M. Sanchez-Sanchez, A. Trunschke, R. Schlögl, M. Eichelbaum, J. Phys. Chem. C 117 (2013) 26988–26997.
[37] J. Schumann, M. Eichelbaum, T. Lunkenbein, N. Thomas, M.C. Alvarez Galvan, R. Schlögl, M. Behrens, ACS Catal. 5 (2015) 3260–3270.
[38] J.C. Slater, Rev. Mod. Phys. 18 (1946) 441–512.
[39] I.M. Hamadeh, P.R. Griffiths, Appl. Spectrosc. 41 (1987) 682–688.
[40] T. Armaroli, T. Bécu, S. Gautier, Oil & Gas Sci. Technol. 59 (2004) 215–237.
[41] F. Boccuzzi, A. Chiorino, M. Manzoli, Surf. Sci. 454–456 (2000) 942–946.
[42] M. Mihaylov, H. Knözinger, K. Hadjiivanov, B.C. Gates, Chem. Ing. Tech. 79 (2007) 795–806.
[43] B. Schumacher, Y. Denkwitz, V. Plzak, M. Kinne, R.J. Behm, J. Catal. 224 (2004) 449–462.
[44] C.J. Pursell, B.D. Chandler, M. Manzoli, F. Boccuzzi, J. Phys. Chem. C 116 (2012) 11117–11125.
[45] J. Saavedra, C. Powell, B. Panthi, C.J. Pursell, B.D. Chandler, J. Catal. 307 (2013) 37–47.
[46] U. Diebold, M. Li, O. Dulub, E.L.D. Hebenstreit, W. Hebenstreit, Surf. Rev. Lett. 7 (2000) 613–617.
[47] M. Bowker, P. Stone, P. Morrall, R. Smith, R. Bennett, N. Perkins, R. Kvon, C. Pang, E. Fourre, M. Hall, J. Catal. 234 (2005) 172–181.
[48] H.G. Boyen, G. Kästle, F. Weigl, B. Koslowski, C. Dietrich, P. Ziemann, J.P. Spatz, S. Riethmüller, C. Hartmann, M. Möller, G. Schmid, M.G. Garnier, P. Oelhafen, Science 297 (2002) 1533–1536.
[49] Z. Jiang, W. Zhang, L. Jin, X. Yang, F. Xu, J. Zhu, W. Huang, J. Phys. Chem. C 111 (2007) 12434–12439.
[50] D. Widmann, R.J. Behm, Chin. J. Catal. 37 (2016) 1684–1693.
[51] N. Kruse, S. Chenakin, Appl. Catal. A 391 (2011) 367–376.
[52] J.T. Calla, M.T. Bore, A.K. Datye, R.J. Davis, J. Catal. 238 (2006) 458–467.
[53] Y. Denkwitz, B. Schumacher, G. Kucèrová, R.J. Behm, J. Catal. 267 (2009) 78–88.
[54] D. Widmann, Y. Liu, F. Schüth, R.J. Behm, J. Catal. 276 (2010) 292–305.
[55] D. Cunningham, S. Tsubota, N. Kamijo, M. Haruta, Res. Chem. Interm. 19 (1993) 1–13.
[56] N.M. Gupta, A.K. Tripathi, J. Catal. 187 (1999) 343–347.
[57] H. Liu, A.I. Kozlov, A.P. Kozlova, T. Shido, K. Asakura, Y. Iwasawa, J. Catal. 185 (1999) 252–264.
[58] A.A. Davydov, N. Sheppard, Molecular Spectroscopy of Oxide Catalyst Surfaces, John Wiley & Sons Ltd (2003) 27–179.
[59] J. Baltrusaitis, J. Schuttlefield, E. Zeitler, V.H. Grassian, Chem. Eng. J. 170 (2011) 471–481.
[60] S. Chen, T. Cao, Y. Gao, D. Li, F. Xiong, W. Huang, J. Phys. Chem. C 120 (2016) 21472–21485.
[61] M.A. Bollinger, M.A. Vannice, Appl. Catal. B 8 (1996) 417–443.
[62] P. Konova, A. Naydenov, CV. Venkov, D. Mehandjiev, D. Andreeva, T. Tabakova, J. Mol. Catal. A 213 (2004) 235–240.
[63] M.C. Raphulu, J. McPherson, E. Lingen, J.A. Anderson, M.S. Scurrell, Gold Bull. 43 (2010) 21–28.
[64] L.F. Chen, C.K. Ong, C.P. Neo, V.V. Varadan, V.K. Varadan, Microwave Electronics: Measurement and Materials Characterization, John Wiley & Sons, Ltd, 2004.
[65] B.K. Na, M.A. Vannice, A.B. Walters, Phys. Rev. B 46 (1992) 12266.
[66] U. Balachandran, N.G. Eror, J. Mater. Sci. 23 (1988) 2676–2682.
[67] M.A. Henderson, Surf. Sci. 419 (1999) 174–187.
[68] S. Bonanni, K. Ait-Mansour, W. Harbich, H. Brune, J. Am. Chem. Soc. 134 (2012) 3445–3450.
[69] I.X. Green, W. Tang, M. Neurock, J.T. Yates, Science 333 (2011) 736–739.
[70] Y. Wang, F. Lehnert, D. Widmann, D. Gu, F. Schüth, R.J. Behm, Angew. Chem. Int. Ed. (2017), http://dx.doi.org/10.1002/anie.201702178.
[71] B.K. Chang, B.W. Jang, S. Dai, S.H. Overbury, J. Catal. 236 (2005) 392–400.
[72] G. Martra, Appl. Catal. A 200 (2000) 275–285.
[73] W. Su, J. Zhang, Z. Feng, T. Chen, P. Ying, C. Li, J. Phys. Chem. C 112 (2008) 7710–7716.
[74] M. Boronat, P. Concepción, A. Corma, J. Phys. Chem. C 113 (2009) 16772–16884.
[75] D.A. Panayotov, V.A. Burrows, J.T. Yates Jr., L. Morris, J. Phys. Chem. C 115 (2011) 22400–22408.

[76] I.X. Green, W. Tang, M. McEntee, M. Neurock, J.T. Yates, J. Am. Chem. Soc. 134 (2012) 12717–12723.
[77] A. Fielicke, G. van Helden, G. Meijer, B. Simard, D.M. Rayner, J. Phys. Chem. B 109 (2005) 23935–23940.
[78] M. Daté, H. Imai, S. Tsubota, M. Haruta, Catal. Today 122 (2007) 222–225.
[79] T. Diemant, Z. Zhao, H. Rauscher, J. Bansmann, R.J. Behm, Top. Catal. 44 (2007) 83–93.
[80] G. Busca, H. Saussey, O. Saur, J.C. Lavalley, V. Lorenzelli, Appl. Catal. 14 (1985) 245–260.
[81] L. Yi, G. Ramis, G. Busca, V. Lorenzelli, J. Mater. Chem. 4 (1994) 1755–1761.
[82] L.F. Liao, C.F. Lien, D.L. Shieh, M.T. Chen, J.L. Lin, J. Phys. Chem. B 106 (2002) 11240–11245.
[83] M. Okumura, J.M. Coronado, J. Soria, M. Haruta, J. Conesa, J. Catal. 203 (2001) 168–174.
[84] L.B. Xiong, J.-L. Li, B. Yang, Y. Yu, J. Nanomater. 2012 (2012) 9–21.
[85] X. Xin, T. Xu, J. Yin, L. Wang, C. Wang, Appl. Catal. B 176–177 (2015) 354–362.
[86] M.S. Chen, D.W. Goodman, Science 306 (2004) 252–255.
[87] M.S. Chen, D.W. Goodman, Chem. Soc. Rev. 37 (2008) 1860–1870.